J|A|C|S
ARTICLES
Published on Web 11/26/2004

Surface-Bound Porphyrazines: Controlling Reduction Potentials of Self-Assembled Monolayers through Molecular Proximity/Orientation to a Metal Surface

Benjamin J. Vesper,[†] Khalid Salaita,[†] Hong Zong,[†] Chad A. Mirkin,*[,†]
Anthony G. M. Barrett,[‡] and Brian M. Hoffman*[,†]

Contribution from the Department of Chemistry and Institute for Nanotechnology, Northwestern University, Evanston, Illinois 60208, and Imperial College of Science, Technology and Medicine, London, U.K. SW7 2AY

Received August 5, 2004; E-mail: camirkin@chem.northwestern.edu (C.A.M.); bmh@northwestern.edu (B.M.H.)

Abstract: We report the preparation of two novel H_2[pz(A_n;B_{4-n})] porphyrazines (pzs) which were designed to position themselves quite differently when attached to a surface: one to form a standard self-assembled monolayer (SAM) roughly perpendicular to a surface, the other to lie horizontally along a surface. As the former, we synthesized a pz, **1**, where one pyrrole group is functionalized with two thioethers terminated in mercaptides (SR, R = $(CH_2)_3CONH(CH_2)_2S-$), each protected as a disulfide, and $-S-Me$ is attached to the other pyrrole sites; the latter is a pz, **2**, with dialkoxybenzo groups fused to two *trans*-pyrroles of the pz ring, and SR groups are attached to the other pair of pyrroles. Nanostructures of **1** and **2** were successfully patterned on gold surfaces via dip-pen nanolithography, and the predicted molecular orientation of the resulting structures was confirmed by topographic AFM images. The two pzs exhibit similar reduction potentials in solution. Both show large shifts in potential upon surface binding, with the magnitude of the shift depending on the proximity/orientation of the pz to the surface. The first reduction potential of the "vertically" aligned **1** shifts by ca. +430 mV when incorporated in a binary pz/hexanethiol SAM, while that for **2**, which lies flat, shifts by ca. +800 mV; the potential thus shifts by ca. +370 mV upon taking a given pz that stands atop a two-legged insulating "standoff" in a traditional SAM and "laying it down". We suggest these observed effects can be explained by image-charge energetics, and this is supported by a simple model.

Introduction

Interest in the miniaturization and fabrication of nanoscale electronic devices has blossomed in recent years.[1−3] Dip-pen nanolithography (DPN), a relatively new scanning-probe-based nanofabrication technique, enables one to pattern molecules in a controlled manner on a variety of surfaces using an "ink"-coated atomic force microscope (AFM) tip.[4−7] The capillary transport of molecules from the AFM tip to the substrate results in the formations of structures whose sizes can be varied between several hundred nanometers to less than 50 nm in size.[8−10] A significant goal in this field is to prepare lines/patterns that are conducting (i.e., wires), and whose conductivity can be modulated (i.e., devices) as such patterns are of great interest in optical, electrical, and sensing devices.[11−18] Much work has been done to study the intermolecular interactions of self-assembled monolayers (SAMs) prepared for such purposes;[19−27] however, it is still very difficult to accurately predict a priori the properties of surface structures. Small differences

[†] Northwestern University.
[‡] Imperial College of Science, Technology and Medicine.

(1) Alivisatos, A. P. *Science* **1996**, *271*, 933−937.
(2) Cui, Y.; Wei, Q.; Park, H.; Lieber, C. M. *Science* **2001**, *293*, 1289−1292.
(3) Jin, R.; Cao, Y.; Mirkin, C. A.; Kelly, K. L.; Schatz, G. C.; Zheng, J. G. *Science* **2001**, *294*, 1901−1903.
(4) Piner, R. D.; Zhu, J.; Xu, F.; Hong, S.; Mirkin, C. A. *Science* **1999**, *283*, 661−663.
(5) Demers, L. M.; Park, S.-J.; Taton, T. A.; Li, Z.; Mirkin, C. A. *Angew. Chem., Int. Ed.* **2001**, *40*, 3071−3073.
(6) Rozhok, S.; Piner, R.; Mirkin, C. A. *J. Phys. Chem. B* **2003**, *107*, 751−757.
(7) Ginger, D. S.; Zhang, H.; Mirkin, C. A. *Angew. Chem., Int. Ed.* **2004**, *43*, 30−45.
(8) Hong, S.; Zhu, J.; Mirkin, C. A. *Langmuir* **1999**, *15*, 7897−7900.
(9) Hong, S.; Mirkin, C. A. *Science* **2000**, *288*, 1808−1811.
(10) Zhang, H.; Chung, S.-W.; Mirkin, C. A. *Nano Lett.* **2003**, *3*, 43−45.
(11) Loiacono, M. J.; Granstrom, E. L.; Frisbie, C. D. *J. Phys. Chem. B* **1998**, *102*, 1679−1688.
(12) Holdcroft, S. *Adv. Mater.* **2001**, *13*, 1753−1765.
(13) He, H.; Zhu, J.; Tao, N. J.; Nagahara, L. A.; Amlani, I.; Tsui, R. *J. Am. Chem. Soc.* **2001**, *123*, 7730−7731.
(14) Liu, Z. M.; Yasseri, A. A.; Lindsey, J. S.; Bocian, D. F. *Science* **2003**, *302*, 1543−1545.
(15) Walter, E. C.; Zach, M. P.; Favier, F.; Murray, B. J.; Inazu, K.; Hemminger, J. C.; Penner, R. M. *ChemPhysChem* **2003**, *4*, 131−138.
(16) Martin, C. R.; Mitchell, D. T. *Anal. Chem.* **1998**, *70*, 322A−327A.
(17) Fuierer, R. R.; Carroll, R. L.; Feldheim, D. L.; Gorman, C. B. *Adv. Mater.* **2002**, *14*, 154−157.
(18) Basabe-Desmonts, L.; Beld, J.; Zimmerman, R. S.; Hernando, J.; Mela, P.; Garcia Parajo, M. F.; van Hulst, N. F.; van den Berg, A.; Reinhoudt, D. N.; Crego-Calama, M. *J. Am. Chem. Soc.* **2004**, *126*, 7293−7299.
(19) Kuzmenko, I.; Rapaport, H.; Kjaer, K.; Als-Nielsen, J.; Weissbuch, I.; Lahav, M.; Leiserowitz, L. *Chem. Rev.* **2001**, *101*, 1659−1696.
(20) Fendler, J. H. *Chem. Mater.* **2001**, *13*, 3196−3210.
(21) Burtman, V.; Zelichenok, A.; Yitzchaik, S. *Angew. Chem., Int. Ed.* **1999**, *38*, 2041−2045.
(22) Ulman, A. *Chem. Rev.* **1996**, *96*, 1533−1554.
(23) He, Y.; Ye, T.; Borguet, E. *J. Am. Chem. Soc.* **2002**, *124*, 11964−11970.
(24) Zhang, Z.; Hou, S.; Zhu, Z.; Liu, Z. *Langmuir* **2000**, *16*, 537−540.
(25) Yamada, H.; Imahori, H.; Nishimura, Y.; Yamazaki, I.; Ahn, T. K.; Kim, S. K.; Kim, D.; Fukuzumi, S. *J. Am. Chem. Soc.* **2003**, *125*, 9129−9139.

10.1021/ja045270m CCC: $27.50

in the behavior of molecules in a homogeneous medium may become enhanced and extremely prominent in a monolayer. In particular, nanoscale and molecular electronics devices will depend on electron/hole transfer to and/or through molecules in contact or in proximity to metal surfaces,[28] yet there is little information about how molecular proximity/orientation relative to a metal surface influence the properties of surface molecules and molecular structures.[29]

Heteroatom-functionalized porphyrazines (pzs) of the form M[pz(A_n;B_{4-n})], where M represents the incorporated metal ion and A and B represent substituents on a pyrrole, have the potential to be extremely useful as inks for DPN, due in part to their chemical flexibility and robustness.[30] The ability to easily alter the peripheral groups of the pz allows one to control the electronic properties of the compounds,[31−33] while at the same time making them amenable for surface attachment. There are two key elements in the design of M[pz(A_n;B_{4-n})] pz inks: (i) the nature and number of the moieties that attach to the substrate (denoted B) and (ii) the character of "M" and the nature and number of the complementary A peripheral substituents. We show here that by varying the number and position of the B attachments, we can change the proximity/orientation with which a pz binds to the surface. We have prepared pz **1**, designed to "stand up" roughly perpendicular to the surface and form a conventional SAM, and pz **2**, designed to lie "flat" along the surface (Scheme 1). These have been patterned on gold surfaces via DPN, and topographic AFM images confirm that the designed surface structures are realized.

Although there are elegant examples of macrocycles patterned in these two modes,[29,34−39] to our knowledge, there is no prior report which examines the influence of molecular proximity/orientation to a metallic surface in controlling the reduction potentials of a surface nanostructure. Comparison of solution and surface electrochemistry of **1** and **2** reveals large changes in their reduction potentials upon SAM formation on gold. Most intriguingly, although the potentials of **1** and **2** are similar in solution, when **1** is incorporated in a traditional SAM, the two extended surface-attachment linkers of the B group act as an insulating "standoff" between the redox active pz core and the gold surface, and its potential is very different from that of **2**, which is induced to "lie down" through additional surface attachments. Simple calculations suggest these findings can be explained by the dependence of image-charge energetics on molecular proximity/orientation to the metal surface.

Scheme 1. Designed Pz Structures and Monolayer Orientation upon Binding to a Gold Surface

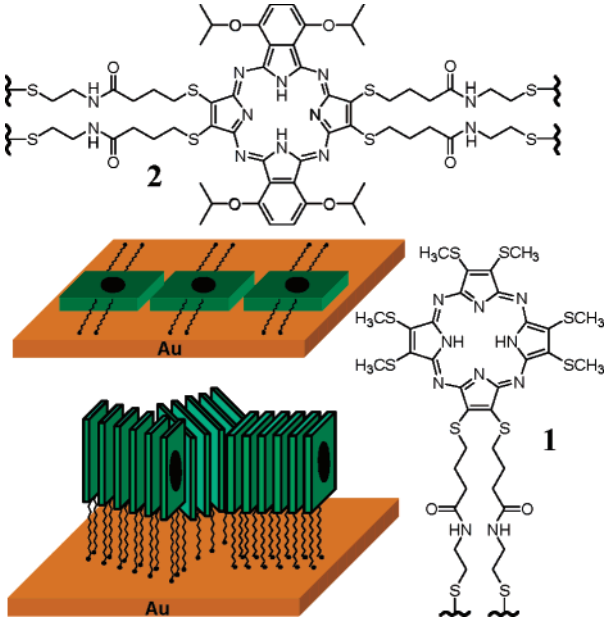

Experimental Section

General Procedures. $[CH_3(CH_2)_3)_4]NPF_6$ (98%), $(CH_3CH_2)_4NBF_4$ (99%), $NaClO_4$ (99%), $NaPF_6$ (99.99%), NH_4PF_6 (99.99%), 2-mercaptoethylamine (95%), 4-methylbenzenethiol (98%), *N*-hydroxysuccinimide (NHS, 97%), and dicyclohexylcarbodiimide (DCC, 99%) were purchased from Aldrich Chemical Co. Ethanol (ACS/USP grade) was purchased from Pharmco Products Inc., and acetonitrile (reagent grade) and methylene chloride (99.9%) were purchased from Fisher Scientific. All chemicals were used as received. Silica gel used for chromatography was Baxter silica gel 60 Å (230−400 mesh). ^{1}H NMR spectra were obtained using a Mercury 400 MHz spectrometer. Matrix-assisted laser desorption ionization time-of-flight mass spectra (MALDI-TOF-MS) were recorded on a PE Biosystems Voyager System 6050, using α-cyano-4-hydroxycinnamic acid as the matrix; electrospray ionization mass spectra (ESI-MS) and atmospheric phase chemical ionization mass spectra (APCI-MS) were recorded using a Micromass Quattro II Electronic HPLC/MS/MS mass spectrometer, and fast atom bombardment mass spectra (FAB-MS) were recorded on a VG-70-250SE high-resolution mass spectrometer. Absorption spectra were recorded using an Agilent 8453 UV-vis spectrophotometer.

Pz Synthesis. 1,2-Dicyano-1,2-bis(methylthio)ethylene ($MNT(Me)_2$, **4**),[40] dimethyl-6,7-dicyano-5,8-dithia-6(*Z*)-dodecenedioate ($MNT(C_4O_2Me)_2$, **5**),[41] 1-imino-4,7-bis(1-methylethoxy)-1,2-benzenedicarbonitrile (diiminoisoindoline, **8**),[42] and pzs **9**, **10**,[41] and **11**[43] were prepared as reported.

(26) Lei, S. B.; Wang, J.; Dong, Y. H.; Wang, C.; Wan, L. J.; Bai, C. L. *Surf. Interface Anal.* **2002**, *34*, 767−771.
(27) Ohshiro, T.; Ito, T.; Buhlmann, P.; Umezawa, Y. *Anal. Chem.* **2001**, *73*, 878−883.
(28) Ratner, M. A.; Ratner, D. *Nanotechnology: a gentle introduction to the next big idea*; Prentice Hall: Upper Saddle River, NJ, 2003.
(29) Yerushalmi, R.; Scherz, A.; van der Boom, M. E. *J. Am. Chem. Soc.* **2004**, *126*, 2700−2701.
(30) Michel, S. L. J.; Baum, S.; Barrett, A. G. M.; Hoffman, B. M. *Prog. Inorg. Chem.* **2001**, *50*, 473−590.
(31) Montalban, A. G.; Jarrell, W.; Riguet, E.; McCubbin, Q. J.; Anderson, M. E.; White, A. J. P.; Williams, D. J.; Barrett, A. G. M.; Hoffman, B. M. *J. Org. Chem.* **2000**, *65*, 2472−2478.
(32) Eichhorn, D. M.; Yang, S.; Jarrell, W.; Baumann, T. F.; Beall, L. S.; White, A. J. P.; Williams, D. J.; Barrett, A. G. M.; Hoffman, B. M. *J. Chem. Soc., Chem. Commun.* **1995**, *16*, 1703−1704.
(33) Baum, S. M.; Trabanco, A. A.; Andres, A.; Montalban, A.; Micallef, A. S.; Zhong, C.; Meunier, H. G.; Suhling, K.; Phillips, D.; White, A. J. P.; Williams, D. J.; Barrett, A. G. M.; Hoffman, B. M. *J. Org. Chem.* **2003**, *68*, 1665−1670.
(34) Zak, J.; Yuan, H.; Ho, M.; Woo, L. K.; Porter, M. D. *Langmuir* **1993**, *9*, 2772−2774.
(35) Gryko, D. T.; Clausen, C.; Roth, K. M.; Dontha, N.; Bocian, D. F.; Kuhr, W. G.; Lindsey, J. S. *J. Org. Chem.* **2000**, *65*, 7345−7355.
(36) Clausen, C.; Gryko, D. T.; Dabke, R. B.; Dontha, N.; Bocian, D. F.; Kuhr, W. G.; Lindsey, J. S. *J. Org. Chem.* **2000**, *65*, 7363−7370.
(37) Hutchison, J. E.; Postlethwaite, T. A.; Murray, R. W. *Langmuir* **1993**, *9*, 3277−3283.
(38) Postlethwaite, T. A.; Hutchison, J. E.; Hathcock, K. W.; Murray, R. W. *Langmuir* **1995**, *11*, 4109−4116.
(39) Hutchison, J. E.; Postlethwaite, T. A.; Chen, C.-h.; Hathcock, K. W.; Ingram, R. S.; Ou, W.; Linton, R. W.; Murray, R. W.; Tyvoll, D. A.; Chng, L. L.; Collman, J. P. *Langmuir* **1997**, *13*, 2143−2148.
(40) Schramm, C. J.; Hoffman, B. M. *Inorg. Chem.* **1980**, *19*, 383−385.
(41) Lee, S.; White, A. J. P.; Williams, D. J.; Barrett, A. G. M.; Hoffman, B. M. *J. Org. Chem.* **2001**, *66*, 461−465.
(42) Forsyth, T. P.; Williams, D. B. G.; Montalban, A. G.; Stern, C. L.; Barrett, A. G. M.; Hoffman, B. M. *J. Org. Chem.* **1998**, *63*, 331−336.
(43) Ehrlich, L. A.; Skrdla, P. J.; Jarrell, W.; Sibert, J. W.; Armstrong, N. R.; Saavedra, S. S.; Barrett, A. G. M.; Hoffman, B. M. *Inorg. Chem.* **2000**, *39*, 3963−3969.

$H_2N(CH_2)_2S_2C_6H_5CH_3$ (3). Commercially available 2-mercaptoethylamine (0.787 g, 0.0102 mol) and 4-methylbenzenethiol (1.51 g, 0.0121 mol) were dissolved in CH_2Cl_2 (120 mL) and MeOH (16 mL). A small chip of iodine was added, and the reaction mixture was stirred overnight at room temperature. After the reaction was complete, the solvent was rotary-evaporated, leaving a yellow oil and a white salt byproduct. The residue was washed in CH_2Cl_2 (120 mL), decanted, and rotary-evaporated to yield **3** (1.57 g, 77.2%) as a viscous yellow oil. The final product was used without further purification: ESI-MS *m*/*z* 200.0 ($M + H^+$) calcd for $C_9H_{13}NS_2$ 199.0.

H_2[Pz((SMe)$_2$)$_3$; ($SC_4O_2Bu)_2$] (6). Mg turnings (0.073 g, 2.99 mmol) and I_2 (0.01 g) in butanol (25 mL) were heated under reflux for 24 h under N_2 to prepare $Mg(OBu)_2$. $MNT(Me)_2$ (**4**; 0.635 g, 3.73 mmol) and $MNT(C_4O_2Me)_2$ (**5**; 0.335 g, 1.06 mmol) were added, and the suspension was heated under reflux for 12 h, during which time the solution turned purple-black. The solvent was distilled off under reduced pressure, and the residue was dissolved in a mixture of CH_2Cl_2 (125 mL) and MeOH (5 mL). Acetic acid (15 mL) was added, and the solution was stirred overnight at room temperature. The mixture was neutralized with NH_4OH, washed with water, dried with $MgSO_4$, and rotary-evaporated. The resulting residue was chromatographed on silica gel (eluent $MeOH/CH_2Cl_2 = 1/99$), yielding the purple solid **6** (25 mg, 10.3%): UV−vis (CH_2Cl_2) λ_{max} (log ϵ) 357 (4.65), 504 (4.32), 635 (4.46), 708 (4.59) nm; APCI-MS *m*/*z* 939.1 ($M + H^+$) calcd for $C_{38}H_{50}N_8O_4S_8$ 938.2.

H_2[Pz((SMe)$_2$)$_3$; ($SC_4O_2H)_2$] (7). Excess LiOH (>2 equiv) in water was added to a solution of **6** (20 mg, 0.021 mmol) in THF (5 mL). The solution was stirred at room temperature for 5 days. The THF was removed by rotary evaporation, and 0.1 M HCl was added dropwise until the solution became acidic. After the mixture was left to stand, a very fine purple solid precipitated. The solid was collected by centrifugation and dried under vacuum to yield **7** in nearly quantitative yield (17 mg, 96.6%): UV−vis (20/80 $MeOH/CH_2Cl_2$) λ_{max} (log ϵ) 352 (4.23), 503 (3.94), 636 (4.07), 706 (4.17) nm; FAB-MS *m*/*z* 827.0 ($M + H^+$) calcd for $C_{30}H_{34}N_8O_4S_8$ 826.0.

H_2[Pz((SMe)$_2$)$_3$; ($SC_4O_2NHC_2S_2PhC$)] (1-TT). Macrocycle **7** (15 mg, 0.018 mmol) and *N*-hydroxysuccinimide (21 mg, 0.18 mmol) were dissolved in 2 mL of THF and cooled in an ice bath. Dicyclohexylcarbodiimide (37 mg, 0.18 mmol) in 1 mL of THF was added with stirring. After 15 min, the mixture was taken out of the ice bath and stirred at room temperature overnight. The mixture was concentrated to dryness and dissolved in CH_2Cl_2. The mixture was filtered, and the solid was washed with CH_2Cl_2. The filtrate and washings were combined, evaporated to dryness under reduced pressure, and dissolved in 5 mL of THF. Disulfide amine **3** (70 mg, 0.35 mmol), dissolved in 5 mL of THF and 10 mL of pH 6.8 buffer, was added, and the mixture was stirred at room temperature overnight. The mixture was concentrated and purified by column chromatography on silica gel (eluent $MeOH/CH_2Cl_2 = 1/99$) to give **1** as a purple solid (15 mg, 69%): UV−vis (CH_2Cl_2) λ_{max} (log ϵ) 352 (4.20), 501 (3.87), 641 (4.00), 709 (4.10) nm; MALDI-TOF-MS *m*/*z* 1188.6 (M^+) calcd for $C_{48}H_{56}N_{10}O_2S_{12}$ 1188.1.

H_2[Pz(A_2); ($SC_4O_2NHC_2S_2PhC)_2$], A = 3,6-Bis(isopropyloxy)-1,2-benzo (2-TT). Pz **2-TT** was prepared analogously to that of **1**, described above, from **10**. From 34 mg of **10** (0.030 mmol), we obtained **2** as a green solid (35 mg, 63%): UV−vis (CH_2Cl_2) λ_{max} (log ϵ) 334 (4.61), 421 (4.26), 648 (4.68), 711 (4.28), 792 (4.60) nm; ^{1}H NMR (400 MHz, $CDCl_3$) δ −0.61 (br s, 2H), 1.80 (d, $J = 6.0$ Hz, 24H), 1.95 (tt, $J = 6.4$ Hz, 8H), 2.20 (s, 12H), 2.52 (m, 16H), 3.27 (d, $J = 6.4$ Hz, 8H), 4.16 (t, $J = 6.0$ Hz, 8H), 5.29 (hp, $J = 6.0$ Hz, 4H), 6.27 (br s, 2H), 6.93 (d, $J = 7.6$ Hz, 8H), 7.14 (d, $J = 8.0$ Hz), 7.58 (s, 4H); ESI-MS *m*/*z* 1843.6 ($M + H^+$) calcd for $C_{88}H_{106}N_{12}O_8S_{12}$ 1842.5.

Dip-Pen Nanolithography and AFM Imaging. DPN of porphyrazines was performed with an atomic force microscope (AFM, CP, Veeco/ThermoMicroscopes, Sunnyvale, CA) equipped with a 100 μm scanner with closed-loop scan control and commercial lithography software (DPNWrite, DPN System-1, NanoInk Inc., Chicago, IL). Gold-coated Si_3N_4 AFM cantilevers (Microlever, Veeco/ThermoMicroscopes, Sunnyvale, CA) with a spring constant of 0.05 N/m were used for patterning and subsequent imaging. Pz-coated tips were prepared by immersing the cantilevers in 1 mM CH_2Cl_2 pz solutions for 5 s and then by blowing the tips dry under a stream of N_2. Substrates were prepared by resistive evaporation of gold (60 nm) on silicon wafers precoated with a 10 nm Ti adhesion layer, as described previously.[44] All DPN patterning experiments were carried out under ambient laboratory conditions (~30% relative humidity, ~20 °C), as previously reported.[4,9,45] Subsequent imaging of the patterned areas was performed under identical conditions (scan rate 4 Hz, contact force 2.5 nN). Tapping-mode images were taken with a Nanoscope IV controller and a NanoMan microscope from Veeco.

Chart 1

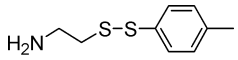

3

Solution Electrochemistry. Cyclic voltammetry measurements were performed at room temperature under nitrogen in dry, deaerated methylene chloride (HPLC grade, Burdick and Jackson) with $[CH_3(CH_2)_3)]_4NPF_6$ (0.1 M) as the supporting electrolyte using a Cypress Systems 2000 electroanalytical system. A three-electrode configuration was employed: a Pt disk working electrode, a Ag wire counter electrode, and a Ag/AgCl (3 M NaCl) reference electrode. Measurements were calibrated by addition of ferrocene as an internal reference, and $E_{1/2}$ values were calculated from $(E_{pa} + E_{pc})/2$ at a scan rate of 110 mV s^{-1}. Pz **11** was also measured in deaerated distilled water using the same three-electrode configuration and $NaPF_6$ (0.5 M) and $NaClO_4$ (1.0 M) as the supporting electrolyte. Potentials were reported versus a ferrocenium/ferrocene couple.[46]

Surface Electrochemistry. Monolayers were prepared on freshly evaporated gold substrates (as described above) by incubating in a CH_2Cl_2 solution containing 1 mM pz for 24 h. Substrates were rinsed with CH_2Cl_2 (three times) and ethanol (three times) to remove any physisorbed material and then dried under a stream of N_2. Monolayer-functionalized gold substrates were placed into an electrochemical cell and used as the working electrode in a three-electrode configuration (Bioanalytical System potentiostat, BAS 100B). The counter electrode was a Pt wire, and all potentials were referenced versus a Ag/AgCl (3 M NaCl) electrode and reported versus a ferrocenium/ferrocene couple. Aqueous solutions of $NaPF_6$ (0.5 M) and $NaClO_4$ (1.0 M) were used as the supporting electrolyte. Scan rates ranging from 25 to 1000 mV s^{-1} were used. Oxygen was not excluded from the cell. Coadsorption studies were carried out by immersing substrates for 24 h in a CH_2Cl_2 solution containing 1 mM pz and 0.4 M hexanethiol.

Results

Porphyrazine Synthesis. To prepare pzs **1** and **2** for surface attachment, a disulfide amine protecting group (**3**; Chart 1) was coupled to the corresponding A_3B or A_2B_2 pz precursor with terminal carboxylic acids (Schemes 2 and 3). Upon application to a gold surface, the weak S−S bonds break, and the pz forms stable thiol−gold surface attachments.

Dip-Pen Nanolithography and AFM Imaging. Porphyrazines **1** and **2** were applied to a polycrystalline gold surface via DPN, characterized by lateral force microscopy (LFM), and the heights of the resulting nanostructures were measured by AFM. The A_3B pz, **1**, was successfully patterned on the surface, as

(44) Weinberger, D. A.; Hong, S.; Mirkin, C. A.; Wessels, B. W.; Higgins, T. B. *Adv. Mater.* **2000**, *12*, 1600−1603.
(45) Hong, S.; Zhu, J.; Mirkin, C. A. *Science* **1999**, *286*, 523−525.
(46) $E(^1/_2)$ (Ag/AgCl) − 0.467 V = $E(^1/_2)$ (Fc^+/Fc)

Scheme 2. Preparation of Thiotoluene (TT)-Protected **1**[a]

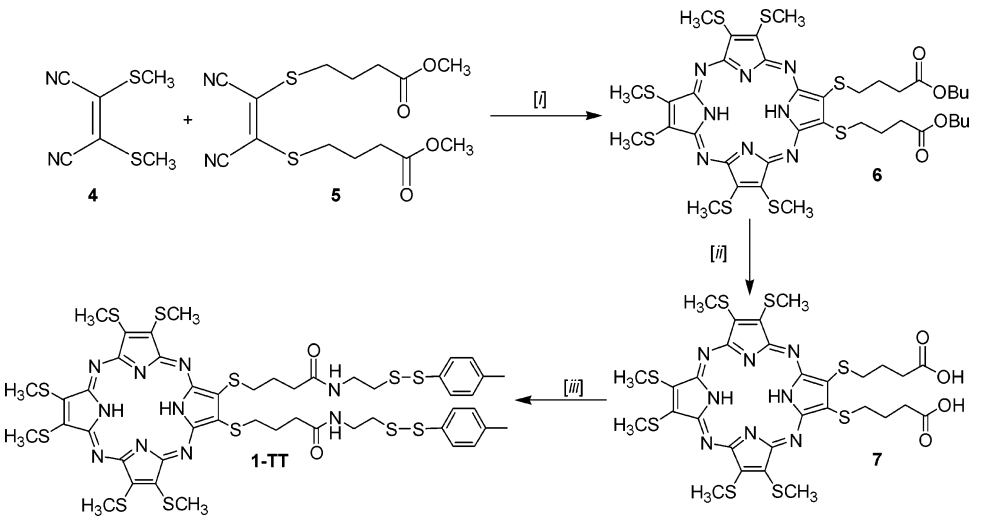

[a] Conditions: [i] (a) $Mg(OBu)_2$, BuOH, reflux; (b) AcOH, NH_4OH. [ii] LiOH, THF/H_2O, 4−5 days. [iii] (a) DCC, NHS, THF; (b) **3**, THF/pH 6.8 buffer.

Scheme 3. Preparation of Thiotoluene (TT)-Protected **2**[a]

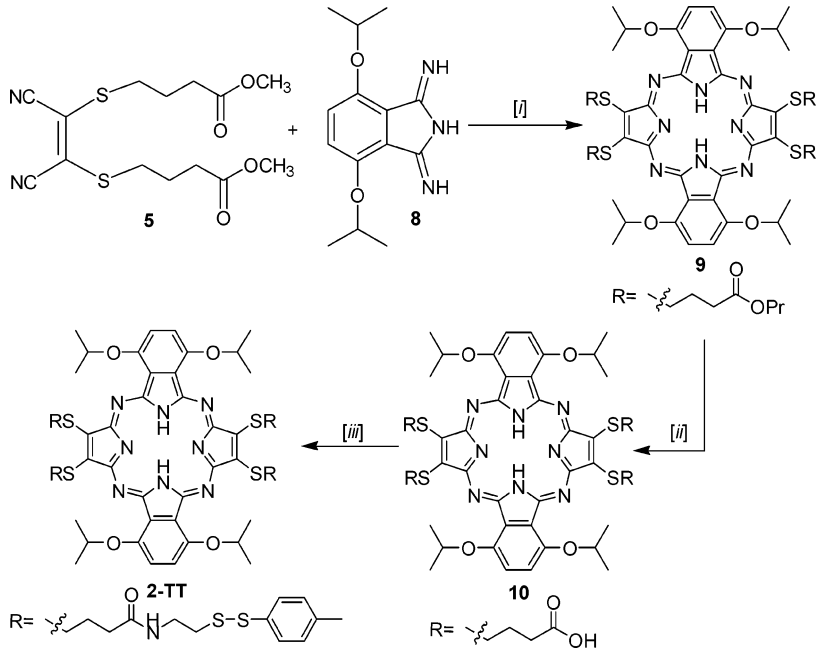

[a] Conditions: [i] (a) $Mg(OPr)_2$, PrOH, reflux; (b) TFA, NH_4OH. [ii] LiOH, THF/H_2O, 4−5 days. [iii] (a) DCC, NHS, THF; (b) **3**, THF/pH 6.8 buffer.

shown by the high friction observed in the LFM image (Figure 1A). The measured topography of ∼3 nm in height mode (Figure 1C) corresponds to those of the pz macrocycle cores that are aligned roughly perpendicular to the surface, forming face-to-face multi-pz structures that are separated from the gold surface by a distance set by the packing of the surface-linking arms (stand off) (Scheme 1). The A_2B_2 pz, **2**, also was successfully patterned, as observed by the LFM image shown in Figure 1B. However, the topographical image of **2** is featureless (Figure 1D), showing that the pz is not elevated above the gold surface, within experimental resolution (∼±1 nm). This indicates that this pz, in fact, binds flat to the surface through the paired disulfide linker groups on each side (Scheme 1).

Electrochemistry. Cyclic voltammetric measurements were carried out on **TT**-protected **1** and **2** dissolved in methylene chloride (Figure 2). The A_3B pz **1** shows two sequential one-electron ring reductions, pz/pz^- ($E_{1/2} = -922$ mV vs Fc^+/Fc) and pz^-/pz^{2-} ($E_{1/2} = -1226$ mV), and a single reversible one-electron ring oxidation, pz^+/pz ($E_{1/2} = 641$ mV), values similar to those of comparable pzs reported earlier.[30] The A_2B_2 pz **2** exhibited only the first ring reduction, pz/pz^- (at −1057 mV), and two sequential one-electron ring oxidations, pz/pz^+ ($E_{1/2} = 253$ mV) and pz^+/pz^{2+} ($E_{1/2} = 583$ mV), again results that are comparable to those for members of this pz subclass.[30] Considering pz/pz^- as the "reporter" couple, the A_3B pz **1** is more easily reduced than **2** by +135 mV. Presumably this difference in potential is attributable to increased electron density of the additional diisopropyloxybenzo ring of **2**, making it more difficult to reduce the pz core.

Monolayers of **1** and **2** were subjected to cyclic voltammetry while immersed in water (Figure 3). The monolayers are quite robust; no changes were noted in films exposed to light and air for weeks, and no changes were observed in the CV of a SAM when scans were repeated up to 30 times. Surface-attached **1**

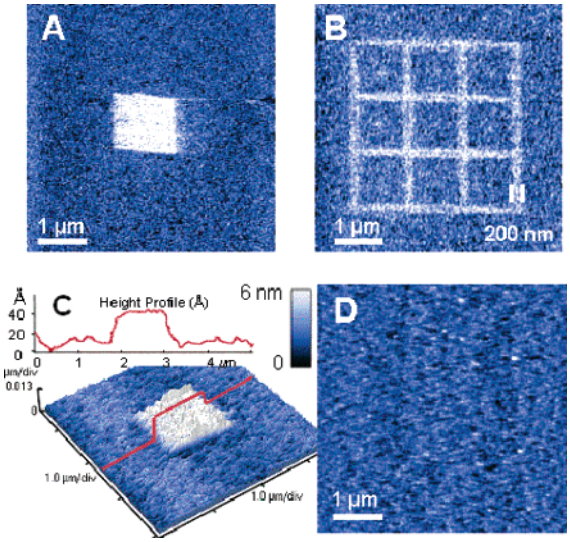

Figure 1. AFM images of porphyrazines **1** and **2** patterned onto a polycrystalline gold surface via dip-pen nanolithography. (A) Lateral force microscopy (LFM) image of a square pattern of **1**. (B) LFM image of a grid pattern of **2**. (C) AFM height image of area shown in A with the averaged height profile of a cross-section. (D) AFM height image of area in B showing no distinctive patterns.

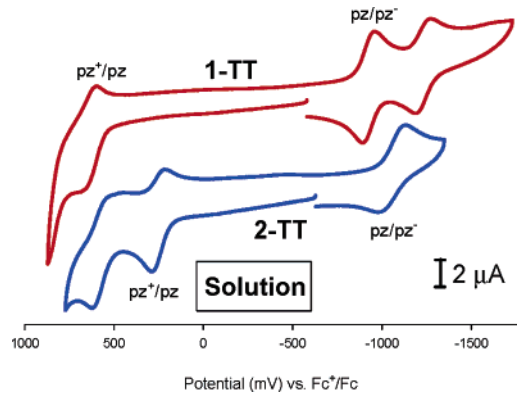

Figure 2. Cyclic voltammograms for **1-TT** and **2-TT** in CH_2Cl_2 solutions with 0.1 M $TBAPF_6$ supporting electrolyte, referenced versus Fc^+/Fc; Ag/AgCl electrode; scan rate = 110 mV s^{-1}.

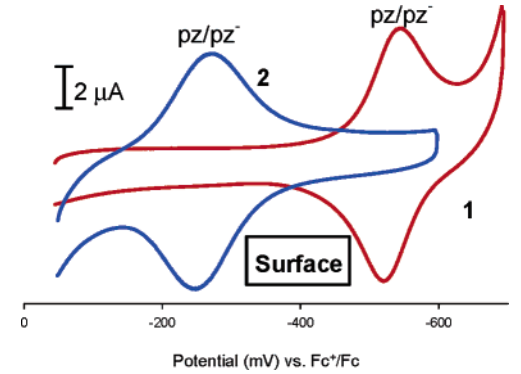

Figure 3. Cyclic voltammograms for SAMs of **1** and **2** on a gold surface with 0.5 M $NaPF_6$ and 1.0 M $NaClO_4$ as supporting electrolyte, reported versus Fc^+/Fc; Ag/AgCl electrode; scan rate = 100 mV s^{-1}.

shows a single ring reduction at −533 mV versus Fc^+/Fc; surface-attached **2** also exhibits a single ring reduction, but it occurs at a much less negative potential, −258 mV.

To obtain the reduction potential for an isolated surface-bound pz, monolayers were prepared in which an excess of hexanethiol as diluent was coadsorbed with the pz. Previous work with

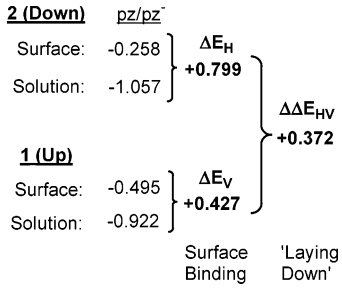

Figure 4. Comparison of the first ring reduction potentials (pz/pz^-, in volts vs Fc^+/Fc) for **1** and **2** in solution (CH_2Cl_2) and as a SAM on a gold surface.

Chart 2

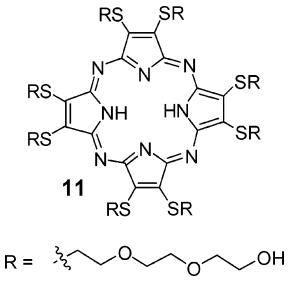

surface-bound ferrocene systems shows that, in some cases, strong intermolecular interactions between surface molecules[47] and/or ion-pairing effects[48] can affect the redox activity of surface centers. Such interactions, in fact, might be anticipated for **1** in a surface monolayer, where the pzs are expected to exhibit significant intermolecular $\pi-\pi$ interactions (Scheme 1). The diluent causes a slight shift (+38 mV) in the ring reduction of **1**; we use the potential for pz **1** in the binary film when comparing surface and solution. The redox couple of a monolayer of **2** was essentially unchanged in a binary film, further evidence that **2** likely lies on the surface.

The shapes of the cyclic voltammograms of SAMs for both pzs are independent of scan rate when scanned from 25 to 1000 mV s^{-1}(Figure S1 of the Supporting Information), while the peak current scales linearly with scan rate (Figure S2 of the Supporting Information). Monolayers of **2** show symmetric redox peaks with a full width at half-maximum (fwhm) of about 91 mV and a peak splitting of about 29 mV at these scan rates; SAMs of **1** show a larger peak splitting, 45 mV, which is reduced to 30 mV when **1** is coadsorbed with hexanethiol.

As the solution pzs are dissolved in methylene chloride, whereas the pz surface assemblies are immersed in water, we measured the effect of solvent on the electrochemistry of the pzs by examining an amphiphilic pz[43] that is soluble in both aqueous and organic solvents, **11** (Chart 2). The CV of **11**, dissolved in methylene chloride, exhibits two one-electron ring reductions, pz/pz^- ($E_{1/2}$ = −998 mV vs Fc^+/Fc) and pz^-/pz^{2-} ($E_{1/2}$ = −1374 mV); the CV in water exhibits only the first ring reduction, pz/pz^- (at −908 mV vs Fc^+/Fc) (Figure S3 of the Supporting Information). Thus, the amphiphilic pz is only slightly more easily reduced (+90 mV) in water than in methylene chloride.

Figure 4 compares the solution pz/pz^- potentials with those for the same molecules attached to the Au surface in binary

(47) Campbell, D. J.; Herr, B. R.; Hulteen, J. C.; Van Duyne, R. P.; Mirkin, C. A. *J. Am. Chem. Soc.* **1996**, *118*, 10211−10219.
(48) Rowe, G. K.; Creager, S. E. *Langmuir* **1991**, *7*, 2307−2312.

films. The difference between surface and solution potentials for the vertically aligned A_3B pz (ΔE_V) indicates that binding this pz to the surface makes it more easily reduced by $\Delta E_V = +427$ mV. A much larger surface/solution difference is observed for the A_2B_2 pz lying along the surface (ΔE_H); when bound to gold, the A_2B_2 pz is more easily reduced by $\Delta E_H = +799$ mV. The difference between the potentials, $\Delta\Delta E_{HV} = \Delta E_H - \Delta E_V = +372$ mV, represents the extent to which a pz core is more easily reduced when lying parallel to the surface than when it is "upright" and separated from the surface by the linker-arms.

Discussion

We have prepared two porphyrazines that were designed to orient themselves quite differently when attached to a surface. Nanostructures of **1** and **2** were successfully patterned on a Au surface via dip-pen nanolithography, and the predicted molecular orientations of the resulting structures (Scheme 1) were confirmed by topographic images (Figure 1); A_3B pz, **1**, with two disulfide linkers on a single side of the pz core, aligns perpendicularly to a surface; A_2B_2 pz, **2**, with two opposite sides of the pz each containing two disulfide linkers, aligns horizontally to the surface. Electrochemical measurements show that the two pzs exhibit rather similar redox chemistry in solution. Both show large shifts in potential upon surface binding (Figure 4); the first reduction potential of the "vertically" aligned **1** shifts by ca. +430 mV when incorporated in a binary pz/hexanethiol SAM, while that for **2**, which lies flat, shifts by ca. +800 mV. The potential thus shifts by ca. +370 mV upon taking a given pz that stands atop a two-legged insulating standoff in a traditional SAM and "laying it down". If one does not correct for the influence of intermolecular interactions between molecules of **1** in a pure SAM, the shift is larger (+410 mV). While there have been studies of the redox properties of suites of molecules that have differing chemical interactions with a metal surface,[49] to our knowledge, there has been no previous comparison of the reduction potentials of such "standing up" and "lying down" structures prepared on metallic surfaces.

The obvious mechanism for generating such large, differential changes in reduction potential upon binding **1** and **2** to a metallic Au surface is image-charge energetics. In the simplest description of image charges, the metal surface is taken to be a perfect conductor and the adsorbed molecule as a point charge; induced charge within Au would then electrostatically stabilize the reduced molecule by an amount, $E_e = -Q^2/4r_o$ (where $|Q| = 1$ is the added charge and r_o is the distance from the charge to the interface), thereby increasing the reduction potential would increase by $+|E_e|$.[50] In the case of **1**, the pz core is separated from the surface by the long side chain linkers, and the increase in potential is subsequently small; for a point charge at a distance of ca. 2 nm, the increase would be ~+200 mV. In contrast, in the monolayer of **2**, the core of the pz is close to the surface; the reduction potential would increase by ~+0.9 V for introduction of a point charge at a distance of ca. 0.4 nm. The difference in the stabilization energies, thus crudely calculated, is of the correct magnitude to explain the large decrease in the energy needed to reduce the "lying down" A_2B_2 pz than the "standing up" A_3B pz. Detailed computations using accurate molecular wave functions and realistic descriptions of the SAM geometry and of the metal surface will be required to fully describe the molecule−surface interaction.

While current technology enables us to accurately predict the orientation of nanofabricated structures based upon the characteristics of the molecular building blocks making up the structures, it is equally important to understand and predict the electronic properties of the structures if these systems are to become useful as molecular devices. Much more comprehensive understanding of these phenomena is needed, and to this end, we are extending this work with studies of other pzs, including analogues of **1**and **2** that have linkers of different lengths, as well as through computational studies of pz−surface interactions.

Acknowledgment. This work has been supported by the National Science Foundation (Grant CHE-0091364) and the Materials Research Center of Northwestern University. The authors thank Professors Mark Ratner and Richard Van Duyne for helpful discussions.

Supporting Information Available: Cyclic voltammograms at varying scan rates, scan rates versus peak current measurements for SAMs of **1** and **2**, and cyclic voltammograms of **11**. This material is available free of charge via the Internet at http://pubs.acs.org.

JA045270M

(49) Zapien, D. C.; Gui, J. Y.; Stern, D. A.; Hubbard, A. T. *J. Electroanal. Chem.* **1992**, *330*, 469−487.

(50) Chen, C. J. *Introduction to scanning tunneling microscopy*; Oxford University Press: New York, 1993.